cAMP/PKA signaling and RIM1α mediate presynaptic LTP in the lateral amygdala

Elodie Fourcaudot*†, Frédéric Gambino†, Yann Humeau*†, Guillaume Casassus*, Hamdy Shaban*, Bernard Poulain†, and Andreas Lüthi*‡

*Friedrich Miescher Institute for Biomedical Research, CH-4058 Basel, Switzerland; and †Institut des Neurosciences Cellulaires et Intégratives, Université Louis Pasteur and Centre National de la Recherche Scientifique, UMR7168, F-67084 Strasbourg, France

Edited by Thomas C. Südhof, University of Texas Southwestern Medical Center, Dallas, TX, and approved August 11, 2008 (received for review July 17, 2008)

NMDA receptor-dependent long-term potentiation (LTP) of glutamatergic synaptic transmission in sensory pathways from auditory thalamus or cortex to the lateral amygdala (LA) underlies the acquisition of auditory fear conditioning. Whereas the mechanisms of postsynaptic LTP at thalamo–LA synapses are well understood, much less is known about the sequence of events mediating presynaptic NMDA receptor-dependent LTP at cortico–LA synapses. Here, we show that presynaptic cortico–LA LTP can be entirely accounted for by a persistent increase in the vesicular release probability. At the molecular level, we found that signaling via the cAMP/PKA pathway is necessary and sufficient for LTP induction. Moreover, by using mice lacking the active-zone protein and PKA target RIM1α (*RIM1*$\alpha^{-/-}$), we demonstrate that RIM1α is required for both chemically and synaptically induced presynaptic LTP. Further analysis of cortico–LA synaptic transmission in *RIM1*$\alpha^{-/-}$ mice revealed a deficit in Ca^{2+}-release coupling leading to a lower baseline release probability. Our results reveal the molecular mechanisms underlying the induction of presynaptic LTP at cortico–LA synapses and indicate that RIM1α-dependent LTP may involve changes in Ca^{2+}-release coupling.

fear conditioning | release probability | synaptic plasticity | synaptic transmission

Auditory fear conditioning requires the induction of NMDA receptor-dependent long-term potentiation (LTP) in the lateral nucleus of the amygdala (LA) (1–3). Sensory information reaches the LA by two main glutamatergic pathways originating in sensory thalamus and cortex (1). The induction and expression of LTP at thalamo–LA synapses is mediated by Ca^{2+} influx through postsynaptic NMDA receptors eventually leading to the recruitment of new AMPA receptors to the postsynaptic membrane (4–7). LTP at cortico–LA synapses is mediated by contrasting mechanisms. Pairing of presynaptic stimulation with postsynaptic depolarization triggers LTP that is induced postsynaptically (5, 8–10) and may involve both pre- and postsynaptic expression mechanisms, such as an increase in glutamate release and the recruitment of postsynaptic AMPA receptors (7–10). In contrast, coactivation of the thalamo– and the cortico–LA pathways results in NMDA receptor-dependent LTP that is induced and expressed entirely via presynaptic mechanisms (10, 11). However, the sequence of molecular events underlying presynaptic cortico–LA LTP is poorly understood.

At the mossy fiber synapse connecting hippocampal granule cells to CA3 pyramidal cells, presynaptic LTP induction does not require NMDA receptor activation, but involves the Ca^{2+}-dependent activation of the cAMP/PKA pathway (12, 13). A similar sequence of events has been demonstrated to underlie presynaptic LTP induction at cerebellar parallel fiber synapses, corticothalamic synapses, and parabrachial afferents to the central amygdala (14–16). One of the key PKA targets necessary for presynaptic LTP is the active-zone scaffolding protein RIM1α (17–19). RIM1α is a multidomain protein that interacts with a number of active-zone proteins involved in neurotransmitter release including Rab3a, Munc13-1, α-liprins, synaptotagmin 1, and presynaptic voltage-dependent Ca^{2+} channels (VDCCs) (19–21).

In the present work, we dissected the physiological and molecular mechanisms underlying the induction and expression of presynaptic cortico–LA LTP. We found that activation of the cAMP/PKA pathway was necessary and sufficient for LTP induction. Downstream of PKA, the presynaptic active-zone protein RIM1α was not only required for LTP, but also for maintaining normal Ca^{2+}-release coupling under baseline conditions. Given that LTP expression was entirely mediated by an increase in the probability of release (P), we conclude that RIM1α-dependent presynaptic LTP at cortico–LA synapses may involve persistent changes in Ca^{2+}-release coupling.

Results

Cortico–LA LTP Increases Probability of Release at a Subset of Synapses. Whole-cell current-clamp recordings from projection neurons showing spike frequency adaptation upon depolarizing current injection were obtained in the dorsal subdivision of the LA (22). Stimulation of afferent fibers from the internal capsule, containing thalamic afferents (1), or from the external capsule, containing cortical afferents (Fig. 1*A*) (1, 23), elicited monosynaptic excitatory postsynaptic potentials (EPSPs) of similar amplitudes and slopes at both inputs. As described (10, 11), simultaneous stimulation of cortico– and thalamo–LA afferents with a single Poisson train (45 stimuli at an average frequency of 30 Hz) resulted in the pathway-specific induction of heterosynaptic associative LTP (LTP_{HA}) at cortico–LA synapses [cortical: $151 \pm 9\%$ of baseline, $n = 14$, $P < 0.01$; thalamic: $108 \pm 4\%$, $n = 14$, not significant (NS)] (Fig. 1*B*). As shown (10), LTP_{HA} was associated with a decrease in the ratio of the postsynaptic responses to double stimulation of cortical afferents (paired-pulse ratio; PPR) ($86 \pm 3\%$ of baseline, $n = 11$, $P < 0.01$) [supporting information (SI) Fig. S1], suggesting a presynaptic expression mechanism.

These observed changes in PPR do not distinguish between the possibilities that LTP_{HA} is entirely mediated by an increase in P at existing release sites, by the recruitment of new release sites with high P, or a mixture of both. Moreover, changes in PPR could also involve postsynaptic mechanisms. We therefore directly assessed changes in P by comparing the time course of NMDA receptor-mediated EPSC block by the activity-dependent open-channel blocker MK-801 (24). Because induction of LTP_{HA} depends on presynaptic, but not postsynaptic,

Author contributions: E.F., Y.H., G.C., B.P., and A.L. designed research; E.F., F.G., Y.H., G.C., and H.S. performed research; E.F., F.G., Y.H., G.C., H.S., B.P., and A.L. analyzed data; and E.F., Y.H., G.C., B.P., and A.L. wrote the paper.

The authors declare no conflict of interest.

This article is a PNAS Direct Submission.

‡To whom correspondence should be addressed at: Friedrich Miescher Institute for Biomedical Research, Maulbeerstrasse 66, CH-4058 Basel, Switzerland. E-mail: andreas.luthi@fmi.ch.

This article contains supporting information online at www.pnas.org/cgi/content/full/0806938105/DCSupplemental.

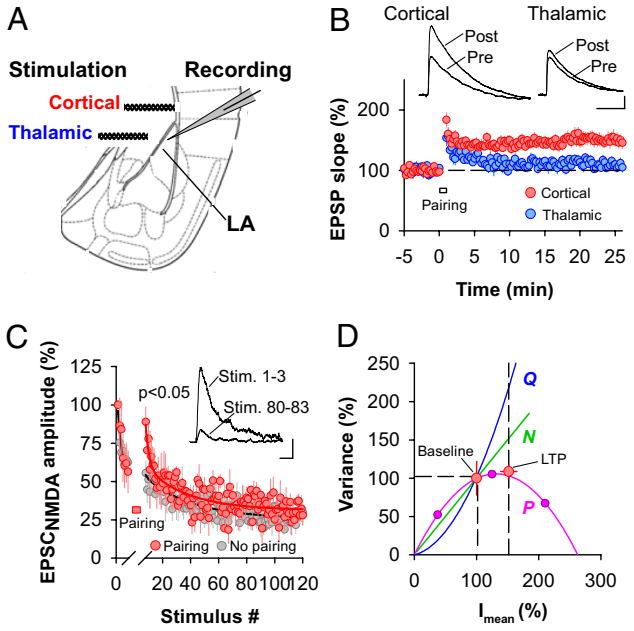

Fig. 1. Presynaptic LTP at cortico–LA synapses is mediated by a persistent increase in the probability of release. (*A*) Placement of stimulating and recording electrodes (LA, lateral amygdala). (*B*) Pathway-specific LTP induction. Simultaneous Poisson train stimulation of the thalamo–LA and cortico–LA pathways induces specific potentiation of cortico–LA synapses ($n = 14$). (Scale bars: 1 mV and 50 ms.) (*C*) Intracellular perfusion with the use-dependent NMDA receptor antagonist MK-801 (1 mM) reveals an increase in *P* after LTP induction. Graph shows the averaged MK-801-induced decay of NMDA receptor-mediated EPSCs before and after LTP induction. Induction of LTP restores a fast-decaying component ($n = 5$). (*Inset*) Traces illustrate the MK-801-induced decline of evoked NMDA receptor-mediated EPSCs. (Scale bars: 10 pA and 50 ms.) (*D*) Variance–mean analysis confirms that LTP at cortico–LA synapses involves an increase in *P*. Comparing EPSC variance before and after LTP induction (red symbols, $n = 7$) with the variance–mean plot obtained by using different Ca^{2+} concentrations ($n = 9$) reveals an almost exclusive increase in *P* after induction of LTP. Green and blue lines indicate the expected increase in variance upon changes in *N* and *Q*, respectively. Error bars, ±SEM.

NMDA receptors (10), MK-801 (1 mM) was intracellularly perfused into the postsynaptic neuron via the patch pipette (10). Subsequently, pharmacologically isolated NMDA-EPSCs were elicited at +30 mV in the presence of NBQX (20 μM). In control experiments, doing so resulted in a gradual decay of the amplitude of NMDA-EPSCs (Fig. 1*C*). The time course of the decay was biphasic and could be fitted with a biexponential function ($\tau_{fast} = 2.3 \pm 0.4$ stimulations; $\tau_{slow} = 29.5 \pm 8.1$ stimulations; $n = 5$) (Fig. 1*C*), indicating that the stimulated synapses exhibited heterogeneous *P*. In a second set of experiments, LTP_{HA} was induced. LTP_{HA} induction resulted in the potentiation of the NMDA-EPSC (158 ± 15%; $n = 5$; Fig. 1*C*). Moreover, LTP_{HA} induction was associated with the reappearance of a fast-decaying component, which had entirely disappeared after the first seven stimulations (Fig. 1*C*). To avoid measuring changes in *P* caused by posttetanic potentiation, stimulation was stopped for 5 min after LTP induction. In principle, the rate of decay of NMDA receptor-mediated currents in the presence of MK-801 can be influenced by postsynaptic mechanisms, such as changes in NMDA receptor mean open time. However, there was no difference in the NMDA-EPSC decay time constants between experimental groups (data not shown), suggesting that LTP induction did not affect NMDA receptor mean open time. Finally, we found the decay of NMDA-EPSCs in the presence of bath-applied MK-801 to be faster in slices in which LTP_{HA} had been induced compared with naïve slices (Fig. S2). Taken together, these experiments indicate that induction of LTP_{HA} results in an increase in *P* at a subset of synapses.

To examine whether this increase in release was mediated by the addition of new functional release sites (*N*) or an increase in average *P* at existing sites, we estimated changes in the number of functional release sites by analyzing the variance to mean amplitude relationship of evoked cortico–LA EPSCs before and after LTP induction. At a given synapse the quantal parameters *N*, *P*, and *Q* can be estimated by analyzing the EPSC variance as a function of the mean amplitude under conditions of different release probabilities (25). When measured at increasing probabilities of release EPSC variance plotted vs. the mean amplitude follows a parabolic function with its initial slope proportional to *Q* and its extent proportional to *N*. We first estimated the baseline quantal parameters of synaptic transmission at cortico–LA synapses at different Ca^{2+} concentrations ($N = 33 \pm 6$; $Q = -7.8 \pm 0.9$ pA; $P_{1mM\ Ca^{2+}} = 0.14 \pm 0.02$; $P_{2.5mM\ Ca^{2+}} = 0.47 \pm 0.08$; $P_{4mM\ Ca^{2+}} = 0.80 \pm 0.01$; $n = 9$) (Fig. 1*D*). In a second set of experiments, the average baseline EPSC variance at 2.5 mM external Ca^{2+} (the Ca^{2+} concentration used in all LTP experiments) was normalized to the parabola obtained from the control experiments by taking into account the $P = f([Ca^{2+}])$ relationship ($n = 7$) (Fig. 1*D*). Subsequently LTP was induced, and the EPSC variance measured after LTP induction was plotted against the increased mean EPSC amplitude, which matched well with the parabola established under control conditions (Fig. 1*D*). Finally, we measured EPSC variance before (at 2.5 mM external Ca^{2+}) and after induction of LTP_{HA} (at three different Ca^{2+} concentrations) in the same neurons. When plotting averaged EPSC variances against mean EPSC amplitudes, all data points fell onto the same parabola (Fig. S3). Together, these findings indicate that expression of LTP_{HA} can entirely be accounted for by an increase in *P*.

To control for the possibility that changes in multivesicular release, which can introduce nonlinearity between the extent in *P* increase and the corresponding enhancement in EPSC amplitude (because of saturation of postsynaptic AMPA receptors), may have led to misinterpretation of the observed changes in *P*, we used the low-affinity AMPA receptor antagonist γ-D-glutamylglycine (γ-DGG), which can be used to probe for changes in synaptic glutamate concentrations that would be expected in the case of increased multivesicular release (26). Comparing the effect of γ-DGG application (2.5 mM) before and after LTP induction revealed no significant difference in the fractional block of AMPA EPSCs (Fig. S4). This indicates that after induction of LTP_{HA} there is no detectable change in synaptic glutamate concentration and in multivesicular release. Thus, estimations of *P* before and after induction of LTP_{HA} are similarly biased.

cAMP/PKA Signaling Is Necessary and Sufficient for Presynaptic LTP Induction. Given the well established role for cAMP/PKA signaling in presynaptic induction of LTP in other brain areas (12–16), we tested whether cAMP/PKA signaling is required for the induction of cortico–LA LTP. We first continuously applied the adenylate cyclase (AC) activator forskolin (FSK; 50 μM), which increased excitatory synaptic transmission at cortical afferents (160 ± 8% of predrug baseline, $n = 5$, $P < 0.05$) (Fig. 2*A*). The persistent increase in synaptic transmission did not require the continuous presence of FSK because a brief pulse (10 min) of FSK had essentially the same effect (148 ± 16% of predrug baseline; $n = 9$; $P < 0.05$) (Fig. S5). Consistent with the idea that FSK potentiates synaptic transmission by enhancing *P*, the increase in EPSP amplitude was correlated with a decrease in PPR (69 ± 11% of predrug baseline, $n = 5$, $P < 0.05$) (Fig. 2*A*). FSK-induced potentiation of synaptic transmission (LTP_{FSK}) completely occluded any further induction of LTP_{HA} by costimulation of thalamo– and cortico–LA afferents (95 ±

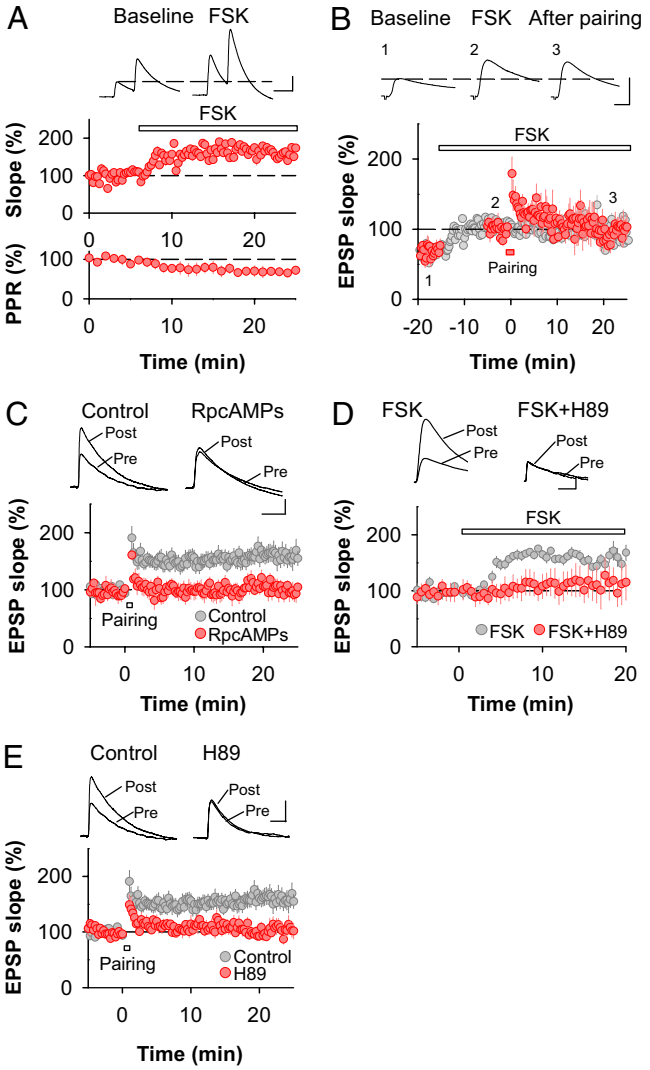

Fig. 2. Activation of the cAMP/PKA pathway is necessary and sufficient for presynaptic LTP. (*A*) Forskolin (50 μM) enhances synaptic transmission ($n = 5$) and decreases PPR ($n = 5$) at cortico-amygdala synapses. (Scale bars: 5 mV and 50 ms.) (*B*) LTP_{FSK} of synaptic transmission occludes the induction of LTP_{HA} ($n = 5$). Gray symbols represent LTP_{FSK} in the absence of LTP_{HA} induction (same data as in *A*). Averaged sample traces were taken at the time points indicated by the numbers. (Scale bars: 5 mV and 10 ms.) (*C*) Induction of LTP_{HA} is blocked by the nonhydrolyzable cAMP analog Rp-cAMPS (100 μM) (control, $n = 18$; Rp-cAMPS, $n = 6$). (Scale bars: 2 mV and 50 ms.) (*D*) LTP_{FSK} requires activation of PKA. Bath application of the PKA antagonist H-89 (20 μM) completely abolishes the effect of FSK on synaptic transmission (control, $n = 5$; H-89, $n = 5$). (Scale bars: 2 mV and 50 ms.) (*E*) Induction of LTP_{HA} at cortico–LA synapses is blocked by the PKA antagonist H-89 (20 μM) (control, $n = 18$; H-89, $n = 8$). (Scale bars: 2 mV and 50 ms.) Error bars, ±SEM.

13% of baseline, $n = 5$, NS) (Fig. 2*B*), suggesting that a rise in presynaptic cAMP mediates LTP_{HA} induction. To test this idea directly, we applied the nonhydrolyzable cAMP analog Rp-adenosine-3′,5′-cyclic monophosphorothioate (Rp-cAMPS) (100 μM). In slices pretreated for 45 min with Rp-cAMPS, cortico–LA LTP could not be induced (control: 160 ± 15% of baseline, $n = 18$, $P < 0.05$; Rp-cAMPS: 101 ± 12% of baseline, $n = 6$, NS) (Fig. 2*C*). This indicates that a rise in cAMP is both necessary and sufficient for induction of LTP_{HA} at cortico–LA synapses.

To assess whether the Rp-cAMPS effect was mediated by PKA, we tested whether the PKA inhibitor H-89 (20 μM) blocked LTP_{FSK} and LTP_{HA}. In the presence of H-89 both

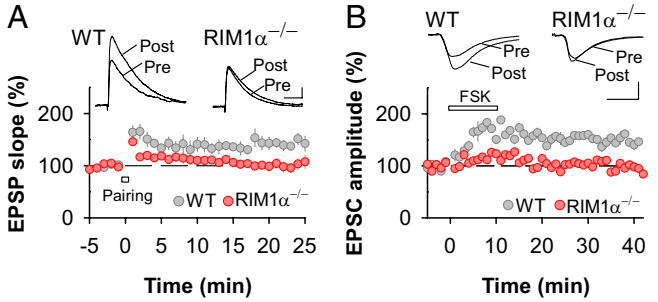

Fig. 3. The PKA target RIM1α is necessary for the induction of presynaptic LTP. (*A*) LTP_{HA} is absent in *RIM1*$\alpha^{-/-}$ mice (wild-type littermates, $n = 5$; *RIM1*$\alpha^{-/-}$, $n = 9$). (Scale bars: 1 mV and 50 ms.) (*B*) LTP_{FSK} is abolished in *RIM1*$\alpha^{-/-}$ mice (50 μM FSK; wild-type littermates, $n = 16$; *RIM1*$\alpha^{-/-}$, $n = 10$). (Scale bars: 100 pA and 10 ms.) Error bars, ±SEM.

LTP_{FSK} (control: 162 ± 14% of baseline, $n = 5$, $P < 0.05$; H-89: 111 ± 29% of baseline, $n = 5$, NS) (Fig. 2*D*) and LTP_{HA} were abolished (control: 160 ± 15% of baseline, $n = 18$, $P < 0.05$; H-89: 103 ± 11% of baseline, $n = 8$, NS) (Fig. 2*E*).

In principle, inhibiting cAMP/PKA signaling could have blocked LTP_{HA} by decreasing synaptic transmission at thalamo–LA synapses, thereby indirectly interfering with the induction process. Because presynaptic cortico–LA LTP becomes independent of thalamic afferent activity, and NMDA receptor activation, if it is induced in the presence of a $GABA_B$ receptor antagonist (11), we examined whether this homosynaptic form of cortico–LA LTP also required cAMP/PKA signaling. Consistent with a direct effect of blockers of the cAMP/PKA signaling pathway on presynaptic cortico–LA LTP, we found that homosynaptic LTP was completely occluded by prior FSK application and blocked by Rp-cAMPS and inhibition of PKA (Fig. S6). This was unlikely mediated by a postsynaptic mechanism because perfusion of the postsynaptic cell with a membrane-impermeable cAMP analog did not interfere with homosynaptic LTP induction (Fig. S6).

Together, these results demonstrate that the increase in P during LTP_{HA} requires the activation of presynaptic AC and PKA and that cAMP/PKA signaling is sufficient for the induction of LTP_{HA}.

The Active-Zone Protein RIM1α Is Necessary for Presynaptic LTP. Next, we addressed the role of the active-zone protein and PKA target RIM1α in LTP_{HA}. LTP_{HA} was completely absent in RIM1α-deficient mice (*RIM1*$\alpha^{-/-}$) (wild-type littermates: 143 ± 10% of baseline, $n = 5$, $P < 0.05$; *RIM1*$\alpha^{-/-}$: 102 ± 10% of baseline, $n = 9$, NS) (Fig. 3*A*). In addition, we examined whether RIM1α was required for LTP_{FSK}, which is completely independent of the thalamo–LA pathway. In accordance with the lack of LTP_{HA}, LTP_{FSK} was abolished in *RIM1*$\alpha^{-/-}$ mice (wild-type littermates: 155 ± 4% of baseline, $n = 16$, $P < 0.05$; *RIM1*$\alpha^{-/-}$: 104 ± 4% of baseline, $n = 10$, NS; measured 25–30 min after FSK application) (Fig. 3*B*).

In contrast to pairing presynaptic stimulation of converging thalamo– and cortico–LA afferents, pairing presynaptic stimulation of cortico–LA afferents with postsynaptic depolarization leads to the simultaneous induction of pre- and postsynaptic LTP at cortico–LA synapses (5, 7). If RIM1α was selectively involved in presynaptic LTP, it should be possible to induce postsynaptic LTP in *RIM1*$\alpha^{-/-}$ mice. Consistent with this hypothesis, we found that in *RIM1*$\alpha^{-/-}$ mice, pairing presynaptic stimulation with postsynaptic depolarization induced LTP of lower magnitude compared with wild-type littermates. In keeping with a postsynaptic locus of expression, the remaining LTP in *RIM1*$\alpha^{-/-}$ mice, in contrast to wild-type littermates, was not

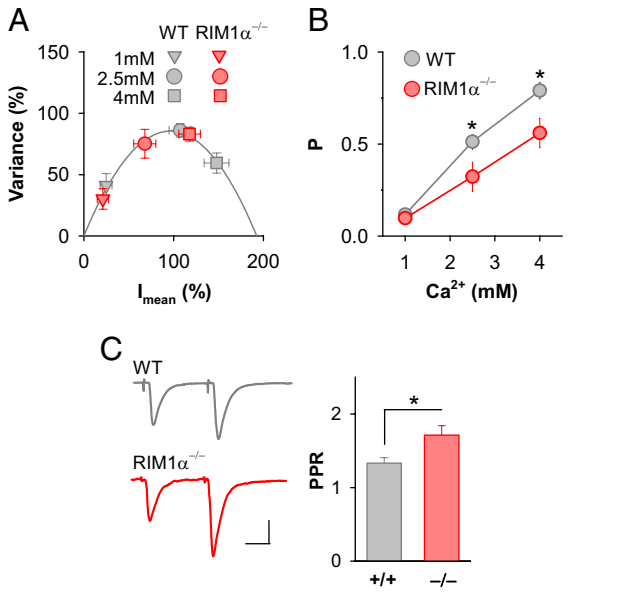

Fig. 4. *RIM1α*$^{-/-}$ mice exhibit decreased baseline release probability. (*A* and *B*) Variance–mean analysis reveals a significantly lower *P* at cortico–LA synapses in *RIM1α*$^{-/-}$ mice. (*A*) Averaged normalized variance–mean plots reveal lower *P* in *RIM1α*$^{-/-}$ mice ($n = 8$) compared with wild-type littermates ($n = 9$). The effect increases with higher external Ca^{2+} concentrations. (*B*) *P* in wild-type mice and *RIM1α*$^{-/-}$ mice plotted as a function of external Ca^{2+} concentration. In *RIM1α*$^{-/-}$ mice, *P* is significantly reduced in 2.5 mM and 4 mM external Ca^{2+}. (*C*) Paired-pulse stimulation reveals altered short-term plasticity in *RIM1α*$^{-/-}$ mice. Consistent with a lower *P*, *RIM1α*$^{-/-}$ mice exhibit an increase in baseline PPR ($n = 7$). (Scale bars: 50 pA and 20 ms.) *, $P < 0.05$. Error bars, ±SEM.

associated with any change in PPR (Fig. S7). Thus, RIM1α is an essential and selective component of the signaling pathway underlying presynaptic LTP induction and/or expression at cortico–LA synapses.

The Active-Zone Protein RIM1α Is Necessary for Normal Ca^{2+}-Release Coupling. That RIM1α is necessary for LTP_{HA} raises the question of whether RIM1α also contributes to *P* during baseline synaptic transmission. Moreover, we wanted to exclude the possibility that the lack of LTP_{HA} in *RIM1α*$^{-/-}$ mice could be explained by occlusion caused by an elevated baseline *P*. Previous studies indicate a role for RIM1α in setting baseline *P* at synapses generally considered not to be competent for expressing RIM1α-dependent presynaptic LTP, such as the Schaffer collateral–CA1 synapse or the neuromuscular junction (27, 28). In contrast, at synapses where RIM1α is necessary for presynaptic LTP, baseline *P*, as measured by short-term synaptic plasticity, does not appear to be affected by the absence of RIM1α (17). To address whether deficiency of RIM1α had an effect on baseline *P* at cortico–LA synapses, we first analyzed *P* at different Ca^{2+} concentrations by using variance-mean analysis (Fig. 4 *A* and *B*). Comparing the relation between EPSC variance and mean EPSC amplitude revealed a significantly lower *P* in *RIM1α*$^{-/-}$ mice ($n = 9$) compared with littermate controls ($n = 8$) (Fig. 4 *A* and *B*). The difference in *P* between wild-type and *RIM1α*$^{-/-}$ mice was increasing as a function of the extracellular Ca^{2+} concentration. Whereas at 1 mM external Ca^{2+} there was no significant difference detectable (wild-type: 0.12 ± 0.02, $n = 9$; *RIM1α*$^{-/-}$: 0.10 ± 0.03, $n = 8$; NS), increasing external Ca^{2+} to 2.5 mM or 4 mM revealed a significant deficit in *P* in *RIM1α*$^{-/-}$ mice (2.5 mM: wild-type: 0.51 ± 0.04, $n = 9$; *RIM1α*$^{-/-}$: 0.32 ± 0.08, $n = 8$; $P < 0.05$ vs. wild-type; 4 mM: wild-type: 0.79 ± 0.04, $n = 9$; *RIM1α*$^{-/-}$: 0.56 ± 0.08, $n = 8$; $P < 0.05$ vs. wild-type) (Fig. 4 *A* and *B*). Thus, although *P* increases in *RIM1α*$^{-/-}$ mice with increasing external Ca^{2+} concentrations, the dependence of *P* on external Ca^{2+} is markedly less pronounced compared with wild-type animals.

The difference in the baseline *P* and in the Ca^{2+} dependence of release in *RIM1α*$^{-/-}$ animals predicts that short-term plasticity should be altered. In keeping with this, we found that the PPR was significantly enhanced in *RIM1α*$^{-/-}$ mice (wild-type PPR: 1.33 ± 0.07; *RIM1α*$^{-/-}$: 1.71 ± 0.13; $n = 7$; $P < 0.05$) (Fig. 4*C*). Thus, at cortico–LA synapses RIM1α appears to play a central role in setting *P* by regulating Ca^{2+}-release coupling.

Discussion

Coactivation of the thalamo– and cortico–LA pathways leads to the induction of associative, NMDA receptor-dependent LTP at cortico–LA synapses. Induction and expression of this form of LTP are exclusively mediated by presynaptic mechanisms (10, 11). In this work, we have examined the sequence of physiological and molecular events underlying its induction and expression. Experiments in the presence of the use-dependent NMDA receptor blocker MK-801 clearly demonstrated that cortico–LA LTP is mediated by an increase in *P*. A more detailed examination of the underlying mechanisms by using variance-mean analysis and application of the low-affinity AMPA receptor antagonist γ-DGG indicated that the number of functional release sites and the contribution of multivesicular release were not affected upon LTP induction. Taken together, we provide strong evidence that the expression of presynaptic cortico–LA LTP is mediated by an increase in the probability of vesicular release at functional release sites.

We found that cAMP/PKA-dependent signaling is necessary and sufficient for the induction of presynaptic LTP at cortico–LA synapses. One of the key PKA target molecules implicated in presynaptic LTP is the active-zone protein RIM1α (17, 18). Whereas a previous study did not find a significant role for RIM1α in cortico–LA LTP induced by tetanic stimulation of cortical afferents alone (29), our present findings demonstrate that RIM1α is necessary for a purely presynaptic form of cortico–LA LTP. In contrast to other synapses, at which cAMP-mediated potentiation of synaptic release has been shown not only to involve RIM1α-dependent processes, but to engage alternative effector pathways (17), cAMP-mediated potentiation of synaptic transmission at cortico–LA synapses was entirely dependent on PKA and RIM1α. Thus, cortico–LA synapses are an ideally suited system to investigate the molecular mechanisms underlying the control of presynaptic short- and long-term plasticity downstream of PKA and RIM1α.

Similar to a previous study examining the role of RIM1α for synaptic transmission at the neuromuscular junction (28), but unlike what has been reported in cultured hippocampal neurons and in the nematode *Caenorhabditis elegans* (30, 31), cortico–LA synapses in *RIM1α*$^{-/-}$ mice exhibited decreased Ca^{2+}-release coupling. Consistent with a role of RIM1α in determining the Ca^{2+} sensitivity of release, we found that *RIM1α*$^{-/-}$ mice exhibited altered short-term synaptic plasticity. Previous studies were unable to identify deficits in baseline release probability at CNS synapses where RIM1α is required for presynaptic LTP (17, 18). This indicates that the downstream effectors of RIM1α may differ between distinct types of glutamatergic synapses and that RIM1α may exert multiple functions involving distinct effector systems.

How could RIM1α mediate presynaptic LTP and determine the Ca^{2+}-release coupling during baseline transmission? Although RIM1α contains C2 domains, which are usually considered to be Ca^{2+}-binding domains, they are degenerated, suggesting that RIM1α does not act itself as a Ca^{2+} sensor (19). RIM1α, however, interacts directly with Ca^{2+}-binding proteins such as Munc13-1 and synaptotagmin 1 (19, 20, 32). Moreover,

RIM1α interacts directly or indirectly with presynaptic VDCCs, thereby regulating the function and/or the physical location of VDCCs in relation to the release site (20, 21, 33). Thus, RIM1α might orchestrate presynaptic signaling complexes and enable compartmentalized signal transduction within presynaptic scaffolds by bringing VDCCs, Ca^{2+} sensors, and the vesicular fusion machinery into close proximity allowing for activity-dependent and persistent modifications in the vesicular release probability.

RIM1$\alpha^{-/-}$ mice exhibit impaired contextual and cued fear conditioning (34). However, given the ubiquitous expression of RIM1α, it is difficult to interpret these findings. Nevertheless, they are consistent with the notion that RIM1α-dependent LTP at cortico–LA synapses might contribute to the acquisition and/or consolidation of fear conditioning. Based on the findings that fear conditioning occludes the subsequent induction of cortico–LA LTP *in vitro* (9) and that cortico–LA LTP induced *in vivo* is very persistent (35), it is tempting to speculate that the behavioral deficits in *RIM1*$\alpha^{-/-}$ mice might be mediated by deficits in presynaptic LTP. Moreover, we have shown that in the absence of presynaptic $GABA_B$ receptor-mediated inhibition, a nonassociative, NMDA receptor-independent form of cortico–LA LTP is unmasked (11). This was associated with a generalization of conditioned fear responses to nonconditioned stimuli, indicating that the balance between associative and nonassociative presynaptic cortico–LA LTP may modulate the degree of fear generalization. It remains to be determined whether loss of presynaptic cortico–LA LTP in *RIM1*$\alpha^{-/-}$ mice affects generalization of conditioned fear. Further experiments using more selective molecular manipulations of defined brain areas or pathways will be required to address these questions.

Materials and Methods

Slice Preparation. Standard procedures were used to prepare 320-μm-thick coronal slices from 3- to 4-week-old male wild-type C57BL/6J, *RIM1*$\alpha^{-/-}$, or littermate control mice following a protocol approved by the Veterinary Department of the Canton of Basel–Stadt (22). Briefly, the brain was dissected in ice-cold artificial cerebrospinal fluid (ACSF), mounted on an agar block, and sliced with a vibratome (Microm-HM650V) at 4°C. Slices were maintained for 45 min at 35°C in an interface chamber containing ACSF equilibrated with 95% O_2/5% CO_2 and containing 124 mM NaCl, 2.7 mM KCl, 2.5 mM $CaCl_2$, 1.3 mM $MgCl_2$, 26 mM $NaHCO_3$, 0.4 mM NaH_2PO_4, 18 mM glucose, and 4 mM ascorbate and then for at least 45 min at room temperature before being transferred to a superfusing recording chamber.

Electrophysiology. Whole-cell recordings from LA projection neurons were performed at 30–32°C in a superfusing chamber. Neurons were visually identified with infrared videomicroscopy by using an upright microscope equipped with a 40× objective. Patch electrodes (3–5 MΩ) were pulled from borosilicate glass tubing and normally filled with a solution containing 120 mM potassium gluconate, 20 mM KCl, 10 mM Hepes, 10 mM phosphocreatine, 4 mM Mg-ATP, and 0.3 mM Na-GTP (pH adjusted to 7.25 with KOH, respectively, 295 mOsm). For voltage-clamp experiments, potassium gluconate and KOH were, respectively, replaced by equimolar cesium gluconate and CsOH. All experiments were performed in the presence of picrotoxin (100 μM). In current-clamp recordings, membrane potential was kept manually at −70 mV. Monosynaptic EPSPs exhibiting constant 10–90% rise times and latencies were elicited by stimulation of afferent fibers with a bipolar twisted platinum/10% iridium wire (25-μm diameter).

Data Acquisition and Analysis. Data were recorded with an Axopatch200B (Molecular Devices), filtered at 2 kHz and digitized at 10 kHz. In all experiments, series resistance was monitored throughout the experiment, and if it changed by >15%, the data were not included in the analysis. Data were acquired and analyzed with pClamp9.2 (Molecular Devices). Changes were quantified by normalizing and averaging EPSC amplitudes or EPSP slopes during the last 5 min of the experiments relative to the 5 min of baseline before LTP induction or drug application. Statistical comparisons were done by using paired or unpaired Student's *t* test as appropriate (two-tailed $P < 0.05$ was considered significant). Variance-mean analysis distinguishes between changes in pre- and postsynaptic quantal parameters (25). For each recording, the release probability *P*, number of functional release sites *N*, and quantum size *Q* were estimated by determining the dependence of EPSC variance on mean amplitude under conditions that alter release. In its simplest form, the relationship between the variance and mean response size can be described as follows: $\mathrm{Var} = N{\cdot}P{\cdot}(1 - P){\cdot}Q^2$, $I_{mean} = N{\cdot}P{\cdot}Q$; thus $\mathrm{Var} = Q{\cdot}I_{\mathrm{mean}} - I_{\mathrm{mean}}{}^2/N$. Variance–$I_{\mathrm{mean}}$ relationships were constructed for steady-state EPSCs evoked in presence of 1, 2.5, and 4 mM extracellular Ca^{2+}. Variance–I_{mean} data were fitted with a least-squares method using the following equation: $y = y0 + ax + bx^2$, where *y* is the variance in EPSC amplitude, *x* is the mean amplitude, and *a* and $-1/b$ refer to estimates of *Q* and *N*, respectively. Other sources of fluctuations than *P* can contribute to EPSC variance, as the quantal intra- and intersite variability and heterogeneity in *P* between release sites, leading to overestimation of *N* and *Q*. For each $\mathrm{Var} = f(I_{\mathrm{mean}})$ plot, maximum Var ($\mathrm{Var}_{\mathrm{max}}$) and corresponding I_{mean} (I_{mean}-to-$\mathrm{Var}_{\mathrm{max}}$) were determined. Data obtained from different slices and animals were pooled by normalization to $\mathrm{Var}_{\mathrm{max}}$ and I_{mean}-to-$\mathrm{Var}_{\mathrm{max}}$. Albeit normalization of Var and I_{mean} data results in the loss of information about the estimates of *N* and *Q*, this representation preserves the evaluation of their relative changes. The normalized $\mathrm{Var} = f(I_{\mathrm{mean}})$ data were also fitted by the equation: $y = y0 + ax + bx^2$. When this relationship is a parabola, $\mathrm{Var}_{\mathrm{max}}$ is reached for $P = 0.5$ as in nonnormalized plots, allowing for determination of *P* at each point of the parabola.

Reagents. Picrotoxin was from Sigma–Aldrich. Forskolin, γ-DGG, H-89, MK-801, NBQX, and Rp-cAMPS were from Tocris Bioscience.

ACKNOWLEDGMENTS. We thank Drs. I. Ehrlich, J. Letzkus, and all members of the Lüthi laboratory for helpful discussions and comments on the manuscript, and T. Südhof (Stanford University, Palo Alto, CA) for *RIM1*$\alpha^{-/-}$ mice. This work was supported by the Agence Nationale pour la Recherche, the European Neuroscience Institutes Network, the Eucor Learning and Teaching Mobility Program, the Swiss National Science Foundation, and the Novartis Research Foundation.

1. LeDoux JE (2000) Emotion circuits in the brain. *Annu Rev Neurosci* 23:155–184.
2. Maren S (2001) Neurobiology of Pavlovian fear conditioning. *Annu Rev Neurosci* 24:897–931.
3. Sigurdsson T, Doyère V, Cain CK, LeDoux JE (2007) Long-term potentiation in the amygdala: A cellular mechanism of fear learning and memory. *Neuropharmacology* 52:215–227.
4. Bauer EP, Schafe GE, LeDoux JE (2002) NMDA receptors and L-type voltage-gated calcium channels contribute to long-term potentiation and different components of fear memory formation in the lateral amygdala. *J Neurosci* 22:5239–5249.
5. Humeau Y, *et al*. (2005) Dendritic spine heterogeneity determines afferent-specific Hebbian plasticity in the amygdala. *Neuron* 45:119–131.
6. Rumpel S, LeDoux J, Zador A, Malinow R (2005) Postsynaptic receptor trafficking underlying a form of associative learning. *Science* 308:83–88.
7. Humeau Y, *et al*. (2007) A pathway-specific function for different AMPA receptor subunits in amygdala long-term potentiation and fear conditioning. *J Neurosci* 27:10947–10956.
8. Huang YY, Kandel ER (1998) Postsynaptic induction and PKA-dependent expression of LTP in the lateral amygdala. *Neuron* 21:169–178.
9. Tsvetkov E, Carlezon WA, Benes FM, Kandel ER, Bolshakov VY (2002) Fear conditioning occludes LTP-induced presynaptic enhancement of synaptic transmission in the cortical pathway to the lateral amygdala. *Neuron* 34:289–300.
10. Humeau Y, Shaban H, Bissière S, Lüthi A (2003) Presynaptic induction of heterosynaptic associative plasticity in the mammalian brain. *Nature* 426:841–845.
11. Shaban H, *et al*. (2006) Generalization of amygdala LTP and conditioned fear in the absence of presynaptic inhibition. *Nat Neurosci* 9:1028–1035.
12. Weisskopf MG, Castillo PE, Zalutsky RA, Nicoll RA (1994) Mediation of hippocampal mossy fiber long-term potentiation by cyclic AMP. *Science* 265:1878–1882.
13. Huang YY, Li XC, Kander ER (1994) cAMP contributes to mossy fiber LTP by initiating both a covalently mediated early phase and macromolecular synthesis-dependent late phase. *Cell* 79:69–79.
14. Salin PA, Malenka RC, Nicoll RA (1996) Cyclic AMP mediates a presynaptic form of LTP at cerebellar parallel fiber synapses. *Neuron* 16:797–803.
15. Castro-Alamancos MA, Calcagnotto ME (1999) Presynaptic long-term potentiation in corticothalamic synapses. *J Neurosci* 19:9090–9097.
16. Lopez de Armentia M, Sah P (2007) Bidirectional synaptic plasticity at nociceptive afferents in the rat central amygdala. *J Physiol (London)* 581:961–970.
17. Castillo PE, Schoch S, Schmitz F, Südhof TC, Malenka RC (2002) RIM1α is required for presynaptic long-term potentiation. *Nature* 415:327–330.
18. Lonart G, *et al*. (2003) Phosphorylation of RIM1α by PKA triggers presynaptic long-term potentiation at cerebellar parallel fiber synapses. *Cell* 115:49–60.
19. Südhof TC (2004) The synaptic vesicle cycle. *Annu Rev Neurosci* 27:509–547.
20. Coppola T, *et al*. (2001) Direct interaction of the Rab3 effector RIM with Ca^{2+} channels, SNAP-25, and synaptotagmin. *J Biol Chem* 276:32756–32762.
21. Hibino H, *et al*. (2002) RIM binding proteins (RBPs) couple Rab3-interacting molecules (RIMs) to voltage-gated Ca^{2+} channels. *Neuron* 34:411–423.

22. Bissière S, Humeau Y, Lüthi A (2003) Dopamine gates LTP induction in lateral amygdala by suppressing feedforward inhibition. *Nat Neurosci* 6:587–592.
23. Smith Y, Paré JF, Paré D (2000) Differential innervation of parvalbumin-immunoreactive interneurons of the basolateral amygdaloid complex by cortical and intrinsic inputs. *J Comp Neurol* 416:496–508.
24. Rosenmund C, Clements JD, Westbrook GL (1993) Nonuniform probability of glutamate release at a hippocampal synapse. *Science* 262:754–757.
25. Silver RA, Momiyama A, Cull-Candy SG (1998) Locus of frequency-dependent depression identified with multiple-probability fluctuation analysis at rat climbing fibre Purkinje cell synapses. *J Physiol (London)* 510:881–902.
26. Christie JM, Jahr CE (2006) Multivesicular release at Schaffer collateral–CA1 hippocampal synapses. *J Neurosci* 26:210–216.
27. Schoch S, *et al*. (2002) RIM1α forms a protein scaffold for regulating neurotransmitter release at the active zone. *Nature* 415:321–326.
28. Schoch S, *et al*. (2006) Redundant functions of RIM1α and RIM2α in Ca^{2+}-triggered neurotransmitter release. *EMBO J* 25:5852–5863.
29. Huang YY, *et al*. (2005) Genetic evidence for a protein-kinase-A-mediated presynaptic component in NMDA-receptor-dependent forms of long-term synaptic potentiation. *Proc Natl Acad Sci USA* 102:9365–9370.
30. Calakos N, Schoch S, Südhof TC, Malenka RC (2004) Multiple roles for the active-zone protein RIM1α in late stages of neurotransmitter release. *Neuron* 42:889–896.
31. Koushika SP, *et al*. (2001) A post-docking role for active-zone protein Rim. *Nat Neurosci* 4:997–1005.
32. Betz A, *et al*. (2001) Functional interaction of the active-zone proteins Munc13–1 and RIM1 in synaptic vesicle priming. *Neuron* 30:183–196.
33. Kiyonaka S, *et al*. (2007) RIM1 confers sustained activity and neurotransmitter vesicle anchoring to presynaptic Ca^{2+} channels. *Nat Neurosci* 10:691–701.
34. Powell CM, *et al*. (2004) The presynaptic active-zone protein RIM1α is critical for normal learning and memory. *Neuron* 42:143–153.
35. Doyère V, Schafe GE, Sigurdsson T, LeDoux JE (2003) Long-term potentiation in freely moving rats reveals asymmetries in thalamic and cortical inputs to the lateral amygdala. *Eur J Neurosci* 17:2703–2715.